

# Anyonic phase transitions in the 1D extended Hubbard model with fractional statistics

Martin Bonkhoff,<sup>1,2</sup> Kevin Jägering,<sup>1</sup> Shijie Hu,<sup>1,3</sup> Axel Pelster,<sup>1</sup> Sebastian Eggert,<sup>1</sup> and Imke Schneider<sup>1</sup>

<sup>1</sup>*Physics Department and Research Center OPTIMAS,  
University of Kaiserslautern-Landau, 67663 Kaiserslautern, Germany*

<sup>2</sup>*Theoretische Physik, Univ. Hamburg, Jungiusstr. 9, 20255 Hamburg, Germany*

<sup>3</sup>*Beijing Computational Science Research Center, Beijing 100193, China*

(Dated: October 2, 2024)

We study one-dimensional (1D) lattice anyons with extended Hubbard interactions at unit filling using bosonization and numerical simulations. The behavior can be continuously tuned from Bosonic to Fermionic behavior by adjusting the topological exchange angle  $\theta$ , which leads to a competition of different instabilities. We present the bosonization theory in presence of dynamic gauge fields, which predicts a phase diagrams of four different gapped phases with distinct dominant correlations. Advanced numerical simulations determine and analyze the exact phase transitions between Mott insulator, charge density wave, dimerized state, and Haldane insulator, all of which meet at a multi-critical line in the parameter space of anyonic angle  $\theta$ , onsite interaction  $U$ , and nearest neighbor repulsion  $V$ . Superfluid and pair-superfluid phases are stable in a region of small  $V$ .

*Introduction.* For continuous one-dimensional (1D) systems an exotic particle species interpolating between Bosons and Fermions was first proposed by Leinaas and Myrheim [1, 2]. This concept of anyons has received renewed interest with the implementation by so-called “lattice anyons” [3–17] based on experimental progress to create artificial gauge fields by dynamic manipulations and Floquet driving in ultra-cold gases [15–25] or by Raman assisted coupling [26, 27]. The originally proposed continuous 1D anyons [1] correspond to the limit of low-filling of interacting lattice anyons [13]. However, for unit filling of one particle per site strong lattice effects give rise to a completely different situation, where several broken symmetry phases are possible, which will be the topic of this Letter. This is motivated by the observation that different instabilities have been established for Fermions and Bosons in the 1D extended Hubbard model at unit filling. In particular, the competition of on-site  $U$  and nearest-neighbor  $V$  interactions leads to a possible dimerized (or bond ordered) phase for Fermions [28–31], while for Bosons and small anyonic exchange angle topological string correlations in form of a Haldane insulator (HI) are observed in an intermediate regime [32–35]. This invites the questions for anyons: What is the nature of an intermediate phase as the anyonic exchange phase  $\theta$  is tuned continuously between Bosonic behavior for  $\theta = 0$  to Fermionic behavior for  $\theta = \pi$ ? The goal of this work is to examine the transitions between all different instabilities and determine the dominant correlations as a function of  $\theta$ ,  $U$  and  $V$  at unit filling.

The 1D extended Hubbard model for anyons can be written in standard notation

$$\hat{H} = \sum_l \left[ -J \hat{a}_l^\dagger \hat{a}_{l+1} + \text{H.c.} + \frac{U}{2} \hat{n}_l (\hat{n}_l - 1) + V \hat{n}_l \hat{n}_{l+1} \right]. \quad (1)$$

The anyonic statistics enters via the exchange phase  $\theta$  in the deformed commutation relations on different sites  $l \neq l'$ :  $\hat{a}_l \hat{a}_{l'}^\dagger - e^{i\theta \text{sgn}(l-l')} \hat{a}_{l'}^\dagger \hat{a}_l = 0$ . Via a generalized Jordan-

Wigner transformation  $\hat{a}_l = \hat{b}_l \exp(i\theta \sum_{j < l} \hat{n}_j)$  [6] the anyonic model can be mapped to a bosonic one  $[\hat{b}_{l'}^\dagger, \hat{b}_l] = 0$  for  $l \neq l'$  with density-dependent hopping

$$\hat{H}_{\text{kin}} = -J \sum_l \left[ \hat{b}_l^\dagger \hat{b}_{l+1} e^{i\theta \hat{n}_l} + \text{H.c.} \right] \quad (2)$$

The on-site commutator  $l = l'$  depends on the physical implementation, which is typically spinless bosons restricted to a maximum of two particles per site [7]. The limit of  $\theta = \pi$  corresponds to spinless “pseudo-Fermions” with the same on-site behavior but anti-commutation relations for  $l \neq l'$ . We now derive the corresponding low-energy field theory which will allow to draw conclusions about the expected phase transitions.

*Bosonization of gauge fields.* For the constraint of maximally two particles per site at average unit filling, an exact representation can be used in terms of spin-1 operators  $\hat{S}_l^z = -\hat{n}_l + 1$  which take on eigenvalues  $-1, 0, 1$  [36]. The operations of the transformed hopping operator are given in terms of spin operators  $\hat{S}_l^+ | -1 \rangle = \sqrt{2} | 0 \rangle$  and  $\hat{S}_l^+ | 0 \rangle = \sqrt{2} | 1 \rangle$  as

$$\hat{H}_{\text{kin}} = -\frac{1}{2} \sum_l \left[ t(\hat{S}_l^z, \hat{S}_{l+1}^z) \hat{S}_l^- \hat{S}_{l+1}^+ + \text{H.c.} \right], \quad (3)$$

where the effective hopping is  $t(-1, 0) = J2e^{i\theta}$ ,  $t(0, 1) = J$ ,  $t(-1, 1) = J\sqrt{2}e^{i\theta}$  and  $t(0, 0) = J\sqrt{2}$ . A similar parametrization for interacting bosons has been used before [33, 37] with the simplification  $t = J$ . Here we keep the full expression for  $t$  to avoid an artificial spin-flip symmetry and implement the  $\theta$ -dependence, which can be written in terms of spin-operators as

$$t(\hat{S}_l^z, \hat{S}_{l+1}^z) = J \left[ 1 + d(\theta) \hat{S}_l^z \right] \left[ 1 + d(0) (\hat{S}_{l+1}^z - 1) \right] \quad (4)$$

with  $d(\theta) = 1 - \sqrt{2}e^{i\theta}$ . Following Refs. [33, 37], we introduce two spin- $\frac{1}{2}$  operators  $\hat{S}_l^- = \hat{S}_{1,l}^- + \hat{S}_{2,l}^-$  and

$\hat{S}_l^z = \hat{S}_{1,l}^z + \hat{S}_{2,l}^z$  for each site. This results in a spin- $\frac{1}{2}$  two-leg ladder model

$$H_{\text{kin}} = -\frac{1}{2} \sum_l \left[ \tilde{t} \left( \hat{S}_{2,l}^z, \hat{S}_{2,l+1}^z \right) \hat{S}_{1,l}^- \hat{S}_{1,l+1}^+ \right. \\ \left. + \tilde{t} \left( \hat{S}_{2,l}^z, \hat{S}_{1,l+1}^z \right) \hat{S}_{1,l}^- \hat{S}_{2,l+1}^+ + 1 \leftrightarrow 2 + \text{H.c.} \right]. \quad (5)$$

with a prefactor  $\tilde{t}(\hat{S}_{i,l}^z, \hat{S}_{j,l+1}^z) \equiv t(\hat{S}_{i,l}^z - 1/2, \hat{S}_{j,l+1}^z + 1/2)$  for  $i, j = 1, 2$ . Note, that the hopping in chain 1 depends on the spin operators  $\hat{S}_{2,l}^z$  in chain 2 and vice versa. In that sense we may speak of a lattice gauge function (see Appendix A)

$$\tilde{t}(\hat{S}_{i,l}^z, \hat{S}_{j,l+1}^z) = \tilde{J} + J_z \hat{S}_{i,l}^z + \bar{J}_z \hat{S}_{j,l+1}^z + J_{zz} \hat{S}_{i,l}^z \hat{S}_{j,l+1}^z \quad (6)$$

with  $\tilde{J} = \frac{J}{4}(1 + \sqrt{2})(1 + \sqrt{2}e^{i\theta})$  and higher spin interaction constants  $J_z = \frac{J}{2}(1 + \sqrt{2})(1 - \sqrt{2}e^{i\theta})$ ,  $\bar{J}_z = \frac{J}{2}(1 - \sqrt{2})(1 + \sqrt{2}e^{i\theta})$ , and  $J_{zz} = J(1 - \sqrt{2})(1 - \sqrt{2}e^{i\theta})$ .

For low energies, the Hamiltonian of the coupled spin chains is expressed in terms of dual bosonic fields  $\Theta_n$  and  $\Phi_n$  for each chain  $n = 1, 2$ , which are defined for a continuum variable normalized such that  $[\Phi_n(x), \Theta_{n'}(x')] = \frac{i}{2} \delta_{n,n'} \text{sgn}(x - x')$  [33]. More details are given in the Appendix B. The resulting Hamiltonian is

$$\hat{H} \simeq \int dx \left[ \sum_{\nu=+,-} \frac{u_\nu}{2} \left( K_\nu (\partial_x \Theta_\nu)^2 + K_\nu^{-1} (\partial_x \Phi_\nu)^2 \right) \right. \\ \left. + \Delta (\partial_x \Theta_+ \partial_x \Phi_+ + \partial_x \Theta_- \partial_x \Phi_-) \right. \\ \left. + g_1 \cos(\sqrt{4\pi}\Phi_+) + g_2 \cos(\sqrt{4\pi}\Phi_-) \right. \\ \left. + g_3 \cos(\sqrt{4\pi}\Theta_-) + g_4 \cos(\sqrt{4\pi}\Phi_-) \cos(\sqrt{4\pi}\Phi_-) \right], \quad (7)$$

which we will discuss below. Here  $\Phi_\pm = \Phi_1 \pm \Phi_2$  and  $\Theta_\pm = (\Theta_1 \pm \Theta_2)/2$  are the fields for the total (+) and relative (-) densities and phases of the two spin- $1/2$  chains. Terms which only affect conserved quantum numbers have been omitted. The parameters in the Hamiltonian can be determined in a weak coupling expansion to first order in  $U, V, J_z, \bar{J}_z$  and  $J_{zz}$

$$K_+ = 2 \left[ 1 + \frac{6V + U - 4\text{Re}J_{zz}/\pi}{\text{Re}(\pi\tilde{J} - J_{zz}/2\pi)} \right]^{-1/2} \quad (8)$$

$$K_- = 2 \left[ 1 + \frac{2V - U - 4\text{Re}J_{zz}/\pi}{\text{Re}(\pi\tilde{J} - J_{zz}/2\pi)} \right]^{-1/2} \quad (9)$$

$$u_\nu = 2a\text{Re}(\tilde{J} - J_{zz}/2\pi^2)/K_\nu \quad (10)$$

$$\Delta = -\frac{a}{\pi} \text{Im}(J_z + \bar{J}_z) = \frac{2Ja}{\pi} \sin\theta \quad (11)$$

$$\frac{g_1}{a} = \frac{1}{2}(2V - U) + \frac{2\text{Re}(J_{zz})}{\pi}, \quad (12)$$

$$\frac{g_2}{a} = \frac{1}{2}(U - 2V) + \frac{2\text{Re}(J_{zz})}{\pi}, \quad (13)$$

$$\frac{g_3}{a} = -\text{Re}(\tilde{J})\pi, \quad (14)$$

$$\frac{g_4}{a} = V - \frac{\text{Re}(J_{zz})}{\pi}, \quad (15)$$

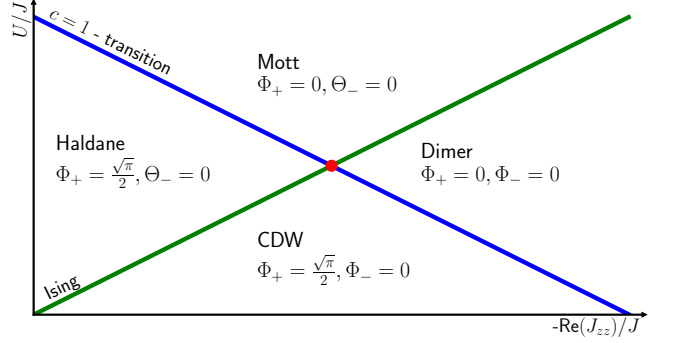


FIG. 1: Schematic phase diagram resulting from Eqs. (16) and (17) for fixed value of  $V$  and  $\tilde{J}$ .

where  $a$  is the lattice constant. The dependence on the anyonic angle  $\theta$  via  $\tilde{J}, J_z, \bar{J}_z, J_{zz}$  comes from an operator product expansion of the density-dependent hopping terms as discussed in the Appendix B. It must be noted here, that the mapping from bosons to spin operators already implies a finite interaction  $J_{zz} \neq 0$  even for  $\theta = U = V = 0$ . Therefore, the weak coupling limit is never exact and the actual coupling constants will quantitatively differ from the formulas given above. Nonetheless, the operator content and the qualitative behavior with increasing  $\theta, V$  and  $U$  is robust.

For  $\theta = 0$  and  $\tilde{t} = J$  we recover the structure and phases for Bosons as discussed in Ref. [33]. For  $\theta > 0$  we notice the appearance of a characteristic anyonic current-density interaction  $\Delta$  on the second line in the Hamiltonian in Eq. (7). This term is present for any filling and leads to different left- and right-moving velocities [13]. While the corresponding time-dependent correlation functions now show chiral behavior, remarkably the static mode expansions of the fields remain unaffected [13] so scaling dimensions and the renormalization behavior are not changed by  $\Delta$ .

*Phase transitions.* Next, we turn to the cos-interactions  $g_1, g_2, g_3, g_4$  on the last two lines of the Hamiltonian (7), all of which may be relevant and lead to gapped phases, depending on  $K_\nu$  [33]. Notably, however, the  $\sin\sqrt{4\pi}\Phi_+$  term is absent, even though spatial inversion symmetry  $\mathcal{I}$  is broken [33]. This is due to the fact, that a modified inversion symmetry  $\tilde{\mathcal{I}}$  is still obeyed as discussed in Ref. [8], which forbids this operator (see Appendix C for a discussion of symmetries).

In the (+) sector a pinning of the field  $\Phi_+$  may occur due to the  $g_1$ -interaction, which is relevant for all repulsive interactions  $K_+ < 2$ . For  $g_1 < 0$  the renormalization flow fixes the value of  $\Phi_+ = 0$ , while it becomes  $\Phi_+ = \sqrt{\pi}/2$  for  $g_1 > 0$ , with a phase transition at  $g_1 = 0$ , characterized by a free field of conformal charge  $c = 1$  [33]. The relative quantum numbers in the (-) channel will also be pinned with long-range correlations. Here, two interactions  $g_2 < 0$  and  $g_3 < 0$  compete with scaling dimensions of  $K_-$  and  $1/K_-$ , respectively. The renormalization flow for  $K_- < 1$  will lead to a minimum at  $\Phi_- = 0$ , while  $K_- > 1$  is characterized by  $\Theta_- = 0$ . The phase transition for  $K_- = 1$  is predicted to be in the

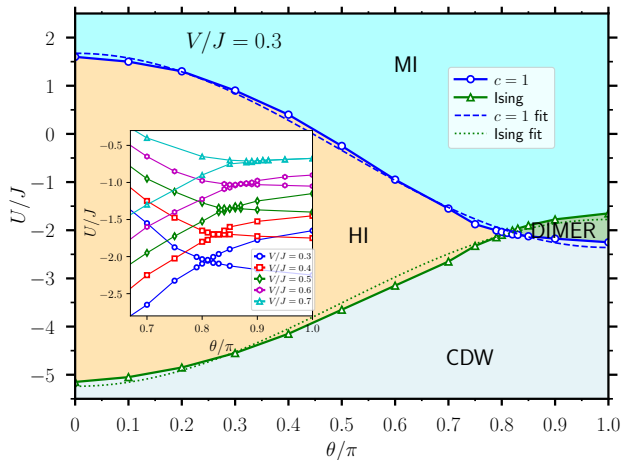


FIG. 2: Phase diagram as a function of  $\theta$  gained by iDMRG (M=400). Inset: Behavior for different  $V$ .

Ising universality class with  $c = 1/2$  as long as  $g_2 \approx g_3$  [33, 39]. For the model at hand a sign change of  $g_2$  is only possible, where it is not the leading instability. The two phase transitions are plotted schematically in Fig. 1 by using the conditions  $g_1 = 0$  and  $K_- = 1$  to determine a critical  $U^c$  as a function of  $-\text{Re}J_{zz} \propto 1 - \sqrt{2} \cos \theta$  for some given value of  $V$ . From Eqs. (8)-(15) we get in the weak-coupling limit

$$U_{c=1}^c(\theta) \sim 2V + \frac{4\text{Re}[J_{zz}(\theta)]}{\pi} \quad (16)$$

$$U_{\text{Ising}}^c(\theta) \sim 2V - \frac{5\text{Re}[J_{zz}(\theta)]}{2\pi} - 3\pi\text{Re}[\tilde{J}(\theta)] \quad (17)$$

For  $\theta = 0$  the corresponding long-range ( $|i - j| \rightarrow \infty$ ) order parameters have been discussed in Ref. [33] in terms of densities  $\delta\hat{n}_l = \hat{n}_l - 1$  and fields: For  $U > U_{c=1}^c > U_{\text{Ising}}^c$  the pinning  $\Phi_+ = \Theta_- = 0$  corresponds to the Mott phase with parity order parameter

$$\mathcal{O}_{\text{MOTT}} = \langle e^{i\pi \sum_{i < k < j} \delta n_k} \rangle \sim \cos \sqrt{\pi} \Phi_+, \quad (18)$$

while  $U_{c=1}^c > U_{\text{Ising}}^c > U$  is a charge density wave (CDW) with alternating charge order  $\Phi_+ = \sqrt{\pi}/2$  and fixed relative densities  $\Phi_- = 0$  corresponding to the order parameter

$$\mathcal{O}_{\text{CDW}} = (-1)^{|i-j|} \langle \delta\hat{n}_i \delta\hat{n}_j \rangle \sim \sin \sqrt{\pi} \Phi_+ \cos \sqrt{\pi} \Phi_-. \quad (19)$$

In the intermediate case,  $U_{c=1}^c > U > U_{\text{Ising}}^c$  a Haldane insulating (HI) phase has been identified with alternating local charge  $\Phi_+ = \sqrt{\pi}/2$  but fluctuating relative densities  $\Theta_- = 0$  and topological string order parameter

$$\mathcal{O}_{\text{HI}} = \langle \delta\hat{n}_i e^{i\pi \sum_{i \leq k < j} \delta\hat{n}_k} \delta\hat{n}_j \rangle \sim \sin \sqrt{\pi} \Phi_+. \quad (20)$$

Now for larger  $\theta$ , anyons open another possibility for the intermediate phase, as  $U_{\text{Ising}}^c$  increases and  $U_{c=1}^c$  decreases with  $\theta$ , such that  $U_{c=1}^c < U < U_{\text{Ising}}^c$ , which is not possible for bosons. In this case the order parameter is

characterized by alternating energies on even and odd bonds

$$\mathcal{O}_{\text{DIMER}} = \langle \hat{H}_{\text{even}}^{\text{bond}} - \hat{H}_{\text{odd}}^{\text{bond}} \rangle \sim \cos \sqrt{\pi} \Phi_+ \cos \sqrt{\pi} \Phi_- \quad (21)$$

corresponding to uniform local charges  $\Phi_+ = 0$  with relative quantum numbers entangled on every second bond  $\Phi_- = 0$ . For the Fermionic Hubbard model the dimer phase is also known as a bond ordered wave [29]. However, it is not trivial that such a phase is now also observed for  $\theta = \pi$  corresponding to "pseudo-Fermions" where the on-site commutator is bosonic with at most two particles per site. The Fermionic Hubbard model has a local Hilbert state of four states per site, while the model in Eq. (1) is restricted to three states, where the relative densities in the  $(-)$  channel play the role of Fermionic spins.

*Numerical results.* The density matrix renormalization group (DMRG) algorithm [40, 41] and the infinite DMRG (iDMRG) [42] were used to calculate the fidelity susceptibility, the entanglement entropy, order parameters and the correlation length, as well as level crossing spectroscopy with finite-size scaling for accurate determination of the phase boundaries. The detailed analysis and data collapse is shown for selected points in the Appendix D, which yield the phase diagrams as shown in Fig. 2 and Fig. 3 illustrating the fate of the HI phase for different values of  $\theta$ . For  $\theta = \pi/2$  the width of the HI phase has considerably decreased and for  $\theta = 3\pi/4$  it is almost gone. For  $\theta = \pi$  then the HI phase is completely replaced by a dimer phase consistent with the prediction by bosonization. For the model at hand, the dimer phase extends to negative  $U$  over a larger region than for the Fermionic Hubbard model [29].

The bosonization results in Eqs. (16) and (17) predict a  $\cos \theta$  dependence of the phase transition lines of the form  $U_{c=1}^c(\theta) - U_{c=1}^c(\frac{\pi}{2}) = a \cos \theta$  and  $U_{\text{Ising}}^c(\theta) - U_{\text{Ising}}^c(\frac{\pi}{2}) = b \cos \theta$ , where the weak coupling expressions evaluate to  $a \sim 0.74$  and  $b \sim -8.5$  with opposite sign. For finite coupling values the prefactors change, but the  $\cos$ -behavior appears to be robust as can be seen by the accurate fits of the phase transition lines in Fig. 2, that are given by  $U_{c=1}^c = -0.34 + 2.02 \cos \theta$  and  $U_{\text{Ising}}^c = -3.51 - 1.73 \cos \theta$ .

The inset of Fig. 2 shows the behavior near the points, where all four phases meet for different  $V$ . For each fixed  $V$ , the phase transition lines cross, which would signal the appearance of a four-critical point between the MI, HI, CDW, and dimer phases. According to bosonization the multi-critical point would have central charge  $c = 3/2$  [43]. All data is consistent with four phases meeting exactly at one multi-critical line in the  $U - V - \theta$  parameter space.

More detailed phase diagrams in the  $U - V$ -parameter space for different  $\theta$  are presented in Fig. 3. An interesting aspect for small values of  $V$  is the appearance of a superfluid (SF) for Bosons and pair-superfluid (PSF) phases for both Bosons and Pseudo-Fermions in the insets of Fig. 3. An analytical description of those phases in terms of bosonization is beyond the scope of the work,

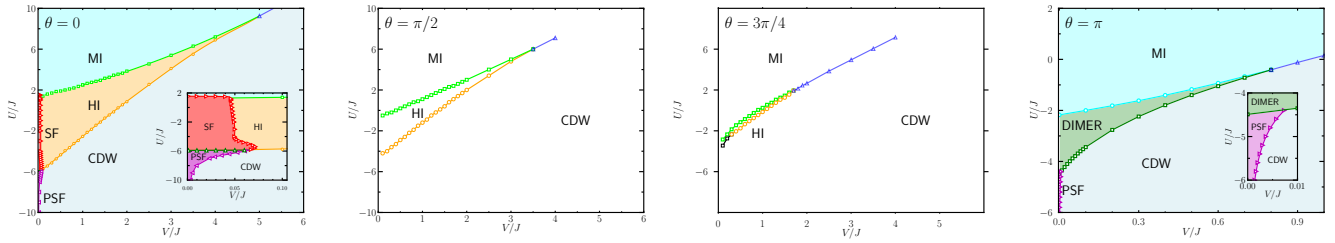


FIG. 3: Phase diagram at  $\theta = 0, \theta = \pi/2, \theta = 3\pi/4$  and  $\theta = \pi$  determined by fidelity susceptibility, correlation length and entanglement peaks from iDMRG ( $M=100-800$ ).

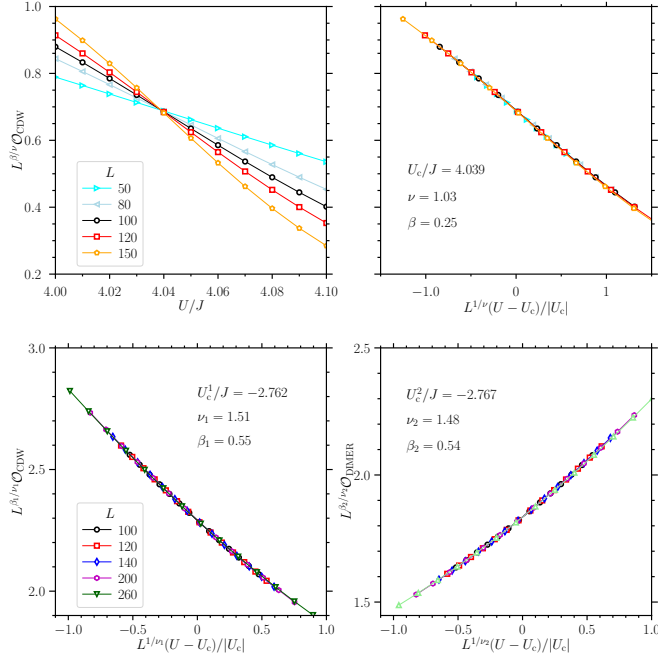


FIG. 4: Data collapse of order parameters at the HI-CDW transition (upper:  $V = 3J, \theta = 0$ ) and the CDW-dimer transitions (lower:  $V = 0.2J, \theta = \pi$ ). Data from DMRG with  $M = 400$ .

however.

*Classification of transitions.* For the determination of universality classes the scaling of the order parameters is analyzed, which is numerically more involved. This is illustrated in Fig. 4(upper) for the transition between the HI and CDW phases. The data collapse gives an accurate determination of critical exponents  $\nu = 1.03$  and  $\beta = .247$ . This is in agreement with the prediction of an Ising transition with  $c = 1/2$  [8, 33], which we confirmed by entanglement entropy scaling [44] also for the dimer to MI transition at large  $\theta$  D.

More interesting is the transition from CDW to dimer phase. Both phases show a spontaneously broken translation symmetry, but different broken inversion symmetries: bond centered and site centered, respectively. Recent literature has extensively discussed continuous transitions between two phases with different broken  $\mathbb{Z}_2$  symmetries as interesting examples [43, 45–54] beyond the Landau-Ginzburg paradigm [55] in connection with

deconfined quantum criticality [52–54]. For the anyon model we can confirm that the CDW-dimer transition also falls in this remarkable category. It is continuous with critical exponents close to  $\nu = 1.5$  and  $\beta = 0.5$  for a  $c = 1$  transition as shown in Fig. 4(lower).

For the extended Bose Hubbard model, the HI to Mott transition is known to be  $c = 1$  [34, 35, 56]. It is weaker for small  $V$  [8] (see Appendix D) and merges to a first order Mott-CDW transition for large  $V$ . We observe no significant change in the nature of the transition for finite  $\theta$ . A coupling in form of the operator  $\sin \sqrt{4\pi} \Phi_+$  is therefore always absent, which would otherwise lead to a crossover behavior instead of the entire  $c = 1$  line [33].

Finally, all transitions between SF/PSF and gapped phases appear to be of Berezinskii-Kosterlitz-Thouless type, independent of  $\theta$ . The corresponding transition lines were established using level crossing spectroscopy starting with exact diagonalization of small systems to identify the relevant energy levels, followed by multi-targeting DMRG simulations up to  $L = 32$  extrapolated to the thermodynamic limit.

*Conclusions.* By derivation of the effective field theory and large scale numerical DMRG calculations we have obtained the phase diagram as a function of  $\theta, U$  and  $V$  of the extended anyonic Hubbard model including negative onsite interactions. The phase diagram consists of four gapped and two superfluid phases. By tuning the exchange angle  $\theta$  from 0 to  $\pi$  the behavior changes continuously from bosonic to fermionic. In the process the Haldane insulator phase disappears at an interesting multicritical point where it is replaced by the dimer phase. The transition between dimer and CDW phases provides an example of a continuous  $c = 1$  transition between two distinct broken  $\mathbb{Z}_2$  symmetries beyond the Ginzburg Landau paradigm.

## ACKNOWLEDGMENTS

We thank Nicholas Sedlmayr, Thore Posske, Sebastian Greschner, Pascal Jung, and Nathan Harshman for helpful discussions. We acknowledge support from the Deutsche Forschungsgemeinschaft (DFG, German Research Foundation) Project No. 277625399-TRR 185 OSCAR (A4,A5,B6) and Forschungsgruppe FOR 2316 (project P10).

## Appendix A: Lattice gauge function

With the restriction of a maximum of two particles per site, the Bosonic creation operator can be expressed exactly in terms of spin-1 operators. In the representation with triplet state of two spin-1/2 operators the final expression is given by

$$\hat{b}_l^\dagger = \frac{\hat{S}_{1,l}^-}{\sqrt{2}} \left( a(0) + d(0)\hat{S}_{2,l}^z \right) + \frac{\hat{S}_{2,l}^-}{\sqrt{2}} \left( a(0) + d(0)\hat{S}_{1,l}^z \right) \quad (\text{A1})$$

where  $a(\theta) = (1 + \sqrt{2}e^{i\theta})/2$  and  $d(\theta) = (1 - \sqrt{2}e^{i\theta})/2$ . We will now derive how this representation is affected by the multiplication with a density dependent phase factor, i.e. we will derive the form of  $\hat{b}_l^\dagger e^{i\theta\hat{n}_l}$ . The density-dependent phase decomposes as  $e^{i\theta(\hat{n}_l-1)} = e^{-i\theta\hat{S}_{1,l}^z} e^{-i\theta\hat{S}_{2,l}^z}$  where the exponentials of spin-1/2 operators can be expressed in terms of trigonometric functions

$$e^{-i\theta\hat{S}_{n,l}^z} = \cos\left(\frac{\theta}{2}\right) \text{id} - 2i \sin\left(\frac{\theta}{2}\right) \hat{S}_{n,l}^z \quad (\text{A2})$$

for  $n = 1, 2$ . We further notice that

$$\left( a(\tilde{\theta}) + d(\tilde{\theta})\hat{S}_{n,l}^z \right) \left( \cos\left(\frac{\theta}{2}\right) - 2i \sin\left(\frac{\theta}{2}\right) \hat{S}_{n,l}^z \right) = e^{-\frac{i\theta}{2}} \left( a(\tilde{\theta} + \theta) + d(\tilde{\theta} + \theta)\hat{S}_{n,l}^z \right) \quad (\text{A3})$$

for arbitrary angles  $\tilde{\theta}$  and  $\theta$ . Multiplication of the Boson operator with the density dependent phase therefore gives

$$\hat{b}_l^\dagger e^{i\theta\hat{n}_l} = \frac{\hat{S}_{1,l}^-}{\sqrt{2}} \left( a(\theta) + d(\theta)\hat{S}_{2,l}^z \right) + \frac{\hat{S}_{2,l}^-}{\sqrt{2}} \left( a(\theta) + d(\theta)\hat{S}_{1,l}^z \right) \quad (\text{A4})$$

In conclusion, on the level of spin-1/2 operators the action of the density dependent phase is solely reflected in the coefficients  $a(\theta)$  and  $d(\theta)$ . This expression also directly yields the lattice gauge function in Eq. (6) of the main text.

## Appendix B: Bosonization

### 1. Mode expansion and Bosonization of spin operators

For the bosonization we follow the standard approach by first using the Jordan-Wigner mapping

$$\hat{S}_{q,l}^+ = \hat{c}_{q,l}^\dagger \exp\left(i\pi \sum_{l' < l} \hat{n}_{q,l'}\right), \quad \hat{S}_{q,l}^z = \hat{n}_{q,l} - \frac{1}{2} \quad (\text{B1})$$

to a Fermionic representation where  $\hat{c}_{q,l}^\dagger$  creates a Fermion on site  $l$  in chain  $q = 1, 2$  and  $\hat{n}_{q,l} = \hat{c}_{q,l}^\dagger \hat{c}_{q,l}$ . We then take the continuum limit and project the Fermionic fields onto states with momentum near the Fermi points  $\pm k_F$ . This leads to right- and left-moving components in the mode expansion:

$$\hat{c}_{q,l} \rightarrow \sqrt{a} \left( \hat{\Psi}_R^q(x) e^{ik_F x} + \hat{\Psi}_L^q(x) e^{-ik_F x} \right) \quad (\text{B2})$$

where  $x = al$  and  $a$  is the lattice constant. Next, we apply the standard Bosonization formula [57]

$$\hat{\Psi}_{R/L}^q(x) = \frac{1}{\sqrt{2\pi a}} e^{i\sqrt{\pi}(\Theta_q(x) \pm \Phi_q(x))} \quad (\text{B3})$$

with the dual Bosonic fields  $\Theta_q$  and  $\Phi_q$  which fulfill  $[\Phi_q(x), \Theta_{q'}(x')] = \frac{i}{2} \delta_{q,q'} \text{sgn}(x - x')$ . Here, the length scale  $a$  also serves as the ultraviolet energy cutoff of the theory. The dual Bosonic fields can be decomposed into right- and left-moving fields  $\Phi_q = \phi_{R,q} + \phi_{L,q}$  and  $\Theta_q = \phi_{R,q} - \phi_{L,q}$ . We use the following mode expansions of these fields

$$\phi_{R,q}(x, t) = \phi_{R,q}^0 + \hat{Q}_{R,q} \frac{x - vt}{L} + \phi_{R,q}^+(x, t) + \phi_{R,q}^-(x, t) \quad (\text{B4})$$

$$\phi_{L,q}(x, t) = \phi_{L,q}^0 + \hat{Q}_{L,q} \frac{x + vt}{L} + \phi_{L,q}^+(x, t) + \phi_{L,q}^-(x, t) \quad (\text{B5})$$



for finite system size  $L$  and periodic boundary conditions where

$$\phi_{R,q}^-(x,t) = (\phi_{R,q}^+(x,t))^\dagger = \sum_n \frac{1}{\sqrt{4\pi n}} e^{i\frac{2\pi n}{L}(x-vt)} b_{R,n}^q \quad (\text{B6})$$

$$\phi_{L,q}^-(x,t) = (\phi_{L,q}^+(x,t))^\dagger = \sum_n \frac{1}{\sqrt{4\pi n}} e^{-i\frac{2\pi n}{L}(x+vt)} b_{L,n}^q . \quad (\text{B7})$$

The Bosonic modes  $b_{R,n}^q$  and  $b_{L,n}^q$  fulfill the canonical commutation relations  $[b_{R/L,n}^q, b_{R/L,n'}^{q\dagger}] = \delta_{n,n'}$  if taken from the same branch, otherwise they commute. The commutation rules for the zero modes are  $[\phi_{R,q}^0, \phi_{L,q}^0] = \frac{i}{4}$  and  $[\phi_{R,q}^0, \hat{Q}_{R,q}] = -\frac{i}{2}$  and  $[\phi_{L,q}^0, \hat{Q}_{L,q}] = \frac{i}{2}$  such that the anti-commutation rules for the Fermion fields are ensured. For the Bosonic fields it follows

$$[\phi_{R/L,q}^-(x,t), \phi_{R/L,q}^+(y,0)] = -\frac{1}{4\pi} \ln \left( 1 - e^{\pm i\frac{2\pi}{L}(x-y \mp vt)} e^{-\frac{2\pi}{L}a} \right) \quad (\text{B8})$$

where we have again used the short distance cutoff  $a$  to generate convergence. Using Baker-Cambell-Hausdorff  $e^A e^B = e^{A+B} e^{\frac{1}{2}[A,B]}$  the vertex operators are normal-ordered:

$$\frac{1}{\sqrt{2\pi a}} e^{i\sqrt{4\pi}\phi_{R/L,q}(x)} = \frac{1}{\sqrt{L}} e^{i\sqrt{4\pi}\phi_{R/L,q}^+(x)} e^{i\sqrt{4\pi}\phi_{R/L,q}^-(x)} . \quad (\text{B9})$$

The spin operator  $S_{q,l}^z = \hat{n}_{q,l} - 1/2 =: \hat{n}_{q,l}$  can now be bosonized using

$$: \hat{n}_{q,l} : \simeq a \left[ \hat{\Psi}_R^{q\dagger}(x) \hat{\Psi}_R^q(x+a) + \hat{\Psi}_L^{q\dagger}(x) \hat{\Psi}_L^q(x+a) + (-1)^{\frac{x}{a}} \left( \hat{\Psi}_R^{q\dagger}(x) \hat{\Psi}_L^q(x) + \hat{\Psi}_L^{q\dagger}(x) \hat{\Psi}_R^q(x) \right) \right] . \quad (\text{B10})$$

For the operator product expansion of two Fermion operators of the same branch we find

$$\begin{aligned} \hat{\Psi}_{R/L}^{q\dagger}(x) \hat{\Psi}_{R/L}^q(x+a) &= \frac{1}{L} : e^{\mp i\sqrt{4\pi}\phi_{R/L,q}(x)} :: e^{\pm i\sqrt{4\pi}\phi_{R/L,q}(x+a)} : \\ &\approx \mp \frac{i}{2\pi a} : e^{\mp i\sqrt{4\pi}(\phi_{R/L,q}(x) - \phi_{R/L,q}(x+a))} : \\ &= \frac{1}{2\pi a} \left[ \mp i + a\sqrt{4\pi} \frac{\partial\phi_{R/L,q}(x)}{\partial x} + a^2\sqrt{\pi} \frac{\partial^2\phi_{R/L,q}(x)}{\partial x^2} \right. \\ &\quad \left. \pm ia^2 2\pi \left( \frac{\partial\phi_{R/L,q}(x)}{\partial x} \right)^2 + \mathcal{O}(a^3) \right] \end{aligned} \quad (\text{B11})$$

whereas the rapidly oscillating product of two Fermion operators of different branches is given by

$$(-1)^{\frac{x}{a}} \left( \hat{\Psi}_R^{q\dagger}(x) \hat{\Psi}_L^q(x) + \hat{\Psi}_L^{q\dagger}(x) \hat{\Psi}_R^q(x) \right) = \frac{(-1)^{\frac{x}{a}}}{2\pi a} e^{-2\pi[\phi_{R,q}^0, \phi_{L,q}^0]} e^{-i\sqrt{4\pi}\Phi_q(x)} + \text{H.c.} \quad (\text{B12})$$

$$= \frac{(-1)^{\frac{x}{a}}}{2\pi a} e^{-i\frac{x}{2}} e^{-i\sqrt{4\pi}\Phi_q(x)} + \text{H.c.} \quad (\text{B13})$$

$$= -\frac{(-1)^{\frac{x}{a}}}{\pi a} \sin 2\sqrt{\pi}\Phi_q(x). \quad (\text{B14})$$

In leading order this results in

$$\hat{S}_{q,l}^z \simeq \frac{a}{\sqrt{\pi}} \frac{\partial\Phi_q(x)}{\partial x} - \frac{(-1)^{\frac{x}{a}}}{\pi} \sin 2\sqrt{\pi}\Phi_q(x) . \quad (\text{B15})$$

For the spin raising operator we get

$$\hat{S}_{q,l}^+ \simeq e^{-i\sqrt{\pi}\Theta_q(x)} [b_1 + b_2(-1)^{\frac{x}{a}} \sin(2\sqrt{\pi}\Phi_q(x))] \quad (\text{B16})$$

where  $b_1$  and  $b_2$  are non-universal constants. Note that the phases in the oscillating terms of Eqs. (B15) and (B16) depend on the treatment of zero modes where other conventions are possible [57].

## 2. Bosonization of hopping with dynamic gauge fields

In this section we determine the bosonized expression for the correlated hopping including the density-dependent phase. Our starting point is the spin-1/2 two-leg ladder model from Eq. (5) in the main text

$$H_{\text{kin}} = -\frac{1}{2} \sum_l \left[ \tilde{t} \left( \hat{S}_{2,l}^z, \hat{S}_{2,l+1}^z \right) \hat{S}_{1,l}^- \hat{S}_{1,l+1}^+ + \tilde{t} \left( \hat{S}_{2,l}^z, \hat{S}_{1,l+1}^z \right) \hat{S}_{1,l}^- \hat{S}_{2,l+1}^+ + 1 \leftrightarrow 2 + \text{H.c.} \right]$$

with the lattice gauge function

$$\tilde{t}(\hat{S}_{i,l}^z, \hat{S}_{j,l+1}^z) = \tilde{J} + J_z \hat{S}_{i,l}^z + \bar{J}_z \hat{S}_{j,l+1}^z + J_{zz} \hat{S}_{i,l}^z \hat{S}_{j,l+1}^z \quad (\text{B17})$$

for  $i, j = 1, 2$  which we have derived in the main text with  $\tilde{J} = \frac{J}{4}(1 + \sqrt{2})(1 + \sqrt{2}e^{i\theta})$  and higher spin interaction constants  $J_z = \frac{J}{2}(1 + \sqrt{2})(1 - \sqrt{2}e^{i\theta})$ ,  $\bar{J}_z = \frac{J}{2}(1 - \sqrt{2})(1 + \sqrt{2}e^{i\theta})$ , and  $J_{zz} = J(1 - \sqrt{2})(1 - \sqrt{2}e^{i\theta})$ . We proceed by first bosonizing the free hopping and the gauge function separately and then performing operator-product expansions between the hopping and the lattice gauge terms whenever necessary. As the lattice gauge function is complex-valued we thereby need to consider the operator product expansions between the hermitian conjugated pairs of the hopping and the lattice gauge explicitly. After the Jordan-Wigner transformation the kinetic energy reads

$$H_{\text{kin}} = -\frac{1}{2} \sum_l \left[ t^* (\hat{n}_{2,l}, \hat{n}_{2,l+1}) \hat{c}_{1,l}^\dagger \hat{c}_{1,l+1} + t^* (\hat{n}_{2,l}, \hat{n}_{1,l+1}) \hat{c}_{1,l}^\dagger \hat{c}_{2,l+1} + 1 \leftrightarrow 2 + \text{H.c.} \right]$$

where

$$t(\hat{n}_{i,l}, \hat{n}_{j,l+1}) = \tilde{J} + J_z : \hat{n}_{i,l} : + \bar{J}_z : \hat{n}_{j,l+1} : + J_{zz} : \hat{n}_{i,l} :: \hat{n}_{j,l+1} : \quad (\text{B18})$$

for  $i, j = 1, 2$  and  $*$  denotes complex conjugation while  $: \dots :$  stands for normal ordering by subtracting the ground state expectation value. The Fermionic bilinears for  $k_F = \frac{\pi}{2}$  are given by

$$\begin{aligned} \hat{c}_{q,l}^\dagger \hat{c}_{q,l+1} &\simeq i a \left[ \hat{\Psi}_R^{q\dagger}(x) \hat{\Psi}_R^q(x+a) - \hat{\Psi}_L^{q\dagger}(x) \hat{\Psi}_L^q(x+a) \right] \\ &\quad - (-1)^{\frac{x}{a}} \left( \hat{\Psi}_R^{q\dagger}(x) \hat{\Psi}_L^q(x+a) - \hat{\Psi}_L^{q\dagger}(x) \hat{\Psi}_R^q(x+a) \right) \end{aligned} \quad (\text{B19})$$

and are bosonized similarly to the local density in the previous subsection. In particular, we use Eq. (B11) to determine the uniform contribution and proceed analogously to Eq. (B14) for the oscillating contribution. The result (before taking the Hermitian conjugate) reads

$$\hat{c}_{q,l}^\dagger \hat{c}_{q,l+1} \simeq \frac{1}{\pi} + i \frac{a}{\sqrt{\pi}} \frac{\partial \Theta_q(x)}{\partial x} - \frac{a^2}{2} \left[ \left( \frac{\partial \Theta_q(x)}{\partial x} \right)^2 + \left( \frac{\partial \Phi_q(x)}{\partial x} \right)^2 \right] - \frac{(-1)^{\frac{x}{a}}}{\pi} \cos(2\sqrt{\pi} \Phi_q(x)). \quad (\text{B20})$$

Note the different phase of the oscillating contribution compared to the local density. For the Bosonization of the gauge function we use  $\hat{n}_{q,l} := \hat{S}_{q,l}^z$  in Eq. (B15) and evaluate the product  $: \hat{n}_{q,l} :: \hat{n}_{q,l+1} :$  by performing further operator product expansions. For the cross terms the following expressions are useful

$$\frac{\partial \Phi_q(x)}{\partial x} \sin(2\sqrt{\pi} \Phi_q(x+a)) \simeq -\sin(2\sqrt{\pi} \Phi_q(x)) \frac{\partial \Phi_q(x+a)}{\partial x} = \frac{1}{\sqrt{\pi} a} \cos(2\sqrt{\pi} \Phi_q(x)) \quad (\text{B21})$$

and

$$\sin(2\sqrt{\pi} \Phi_q(x)) \sin(2\sqrt{\pi} \Phi_q(x+a)) \simeq \frac{1}{2} - a^2 \pi \left( \frac{\partial \Phi_q(x)}{\partial x} \right)^2 - \frac{1}{2} \cos(4\sqrt{\pi} \Phi_q) \quad (\text{B22})$$

Altogether, we find

$$: \hat{n}_{q,l} :: \hat{n}_{q,l+1} : \simeq \frac{a^2}{\pi} \left( \frac{\partial \Phi_q(x)}{\partial x} \right)^2 + \frac{2a(-1)^{\frac{x}{a}}}{\sqrt{\pi} \pi} \frac{\partial \Phi_q(x)}{\partial x} \sin(2\sqrt{\pi} \Phi_q(x+a)) \quad (\text{B23})$$

$$\begin{aligned} &- \frac{1}{\pi^2} \sin(2\sqrt{\pi} \Phi_q(x)) \sin(2\sqrt{\pi} \Phi_q(x+a)) \\ &\simeq \frac{a^2}{\pi} \left( \frac{\partial \Phi_q(x)}{\partial x} \right)^2 + \frac{2(-1)^{\frac{x}{a}}}{\pi^2} \cos(2\sqrt{\pi} \Phi_q(x)) \end{aligned} \quad (\text{B24})$$

$$- \frac{1}{\pi^2} \left( \frac{1}{2} - a^2 \pi \left( \frac{\partial \Phi_q(x)}{\partial x} \right)^2 - \frac{1}{2} \cos(4\sqrt{\pi} \Phi_q) \right)$$

which can be summarized as

$$: \hat{n}_{q,l} : : \hat{n}_{q,l+1} : = -\frac{1}{2\pi^2} + \frac{2a^2}{\pi} \left( \frac{\partial \Phi_q(x)}{\partial x} \right)^2 + \frac{2(-1)^{\frac{x}{a}}}{\pi^2} \cos(2\sqrt{\pi}\Phi_q(x)) + \frac{1}{2\pi^2} \cos(4\sqrt{\pi}\Phi_q) . \quad (\text{B25})$$

The different contributions to the correlated intra-chain hopping

$$\hat{\mathcal{K}}_{l,l+1}^{\text{intra}} \equiv -\frac{1}{2} \left( t^* (\hat{n}_{2,l}, \hat{n}_{2,l+1}) \hat{c}_{1,l}^\dagger \hat{c}_{1,l+1} + t^* (\hat{n}_{1,l}, \hat{n}_{1,l+1}) \hat{c}_{2,l}^\dagger \hat{c}_{2,l+1} + \text{H.c.} \right) \quad (\text{B26})$$

$$= \hat{\mathcal{K}}_{l,l+1}^a + \hat{\mathcal{K}}_{l,l+1}^b + \hat{\mathcal{K}}_{l,l+1}^c \quad (\text{B27})$$

can now be determined by direct multiplication. Here, we have defined

$$\hat{\mathcal{K}}_{l,l+1}^a \equiv -\frac{1}{2} \sum_{q=1,2} \left( \tilde{J}^* \hat{c}_{q,l}^\dagger \hat{c}_{q,l+1} + \text{H.c.} \right) \quad (\text{B28})$$

$$\hat{\mathcal{K}}_{l,l+1}^b \equiv -\frac{1}{2} \sum_{q=1,2} \left[ \hat{c}_{q,l}^\dagger \hat{c}_{q,l+1} (J_z^* : \hat{n}_{\bar{q},l} : + \bar{J}_z^* : \hat{n}_{\bar{q},l+1} : ) + \text{H.c.} \right] \quad (\text{B29})$$

$$\hat{\mathcal{K}}_{l,l+1}^c \equiv -\frac{1}{2} \sum_{q=1,2} \left[ J_{zz}^* \hat{c}_{q,l}^\dagger \hat{c}_{q,l+1} : \hat{n}_{\bar{q},l} : : \hat{n}_{\bar{q},l+1} : + \text{H.c.} \right] \quad (\text{B30})$$

where  $\bar{q} = 1$  if  $q = 2$  and  $\bar{q} = 2$  if  $q = 1$ . Since the evaluation of these terms only involves multiplication of fields with different chain indices we do not need to perform further operator product expansions. We obtain

$$\hat{\mathcal{K}}_{l,l+1}^a = \sum_{q=1,2} \left\{ \frac{a^2 \text{Re}(\tilde{J})}{2} \left[ (\partial_x \Theta_q)^2 + (\partial_x \Phi_q)^2 \right] - \frac{a \text{Im}(\tilde{J})}{\sqrt{\pi}} \partial_x \Theta_q \right\} \quad (\text{B31})$$

$$\hat{\mathcal{K}}_{l,l+1}^b = \sum_{q=1,2} \left[ -\frac{a \text{Re}(J_z + \bar{J}_z)}{\pi \sqrt{\pi}} \partial_x \Phi_q - \frac{a^2}{\pi} \text{Im}(J_z + \bar{J}_z) \partial_x \Theta_q \partial_x \Phi_{\bar{q}} - \frac{\text{Re}(J_z - \bar{J}_z)}{\pi^2} \cos(2\sqrt{\pi}\Phi_q) \sin(2\sqrt{\pi}\Phi_{\bar{q}}) \right] \quad (\text{B32})$$

$$\hat{\mathcal{K}}_{l,l+1}^c = \sum_{q=1,2} \left[ -\frac{2a^2 \text{Re}(J_{zz})}{\pi^2} (\partial_x \Phi_q)^2 + \frac{2 \text{Re}(J_{zz})}{\pi^3} \cos(2\sqrt{\pi}\Phi_q) \cos(2\sqrt{\pi}\Phi_{\bar{q}}) - \frac{\text{Re}(J_{zz})}{2\pi^3} \cos(4\sqrt{\pi}\Phi_q) \right] . \quad (\text{B33})$$

We further introduce '+' and '-' fields

$$\Phi_{\pm} = \Phi_1 \pm \Phi_2, \quad \Theta_{\pm} = (\Theta_1 \pm \Theta_2)/2 \quad (\text{B34})$$

which yields

$$\hat{\mathcal{K}}_{l,l+1}^a = \frac{a^2 \text{Re}(\tilde{J})}{2} \left[ 2(\partial_x \Theta_+)^2 + \frac{1}{2} (\partial_x \Phi_+)^2 + 2(\partial_x \Theta_-)^2 + \frac{1}{2} (\partial_x \Phi_-)^2 \right] - \frac{2a \text{Im}(\tilde{J})}{\sqrt{\pi}} \partial_x \Theta_+ \quad (\text{B35})$$

$$\hat{\mathcal{K}}_{l,l+1}^b = -\frac{a \text{Re}(J_z + \bar{J}_z)}{\pi \sqrt{\pi}} \partial_x \Phi_+ - \frac{a^2 \text{Im}(J_z + \bar{J}_z)}{\pi} [\partial_x \Theta_+ \partial_x \Phi_+ + \partial_x \Theta_- \partial_x \Phi_-] + \frac{\text{Re}(J_z - \bar{J}_z)}{\pi^2} \sin(2\sqrt{\pi}\Phi_+) \quad (\text{B36})$$

$$\hat{\mathcal{K}}_{l,l+1}^c = -\frac{a^2 \text{Re}(J_{zz})}{\pi^2} \left[ (\partial_x \Phi_+)^2 + (\partial_x \Phi_-)^2 \right] + \frac{2 \text{Re}(J_{zz})}{\pi^3} \left[ \cos(2\sqrt{\pi}\Phi_+) + \cos(2\sqrt{\pi}\Phi_-) - \frac{1}{2} \cos(2\sqrt{\pi}\Phi_+) \cos(2\sqrt{\pi}\Phi_-) \right] . \quad (\text{B37})$$

Here, we omitted oscillating terms and contributions of higher order. The additional constant in Eq. (B25) entering  $: \hat{n}_{l,q} : : \hat{n}_{l+1,q} :$  can be absorbed into the hopping amplitude of  $\hat{\mathcal{K}}_{l,l+1}^a$ , i.e.  $\tilde{J} \rightarrow \tilde{J} - J_{zz}/2\pi^2$ . Altogether, the



intra-chain hopping is given by

$$\begin{aligned}
\hat{\mathcal{K}}_{l,l+1}^{\text{intra}} \simeq & \frac{a^2 \text{Re} \left( \tilde{J} - \frac{J_{zz}}{2\pi^2} \right)}{2} \left[ 2 (\partial_x \Theta_+)^2 + \frac{1}{2} (\partial_x \Phi_+)^2 + 2 (\partial_x \Theta_-)^2 + \frac{1}{2} (\partial_x \Phi_-)^2 \right] \\
& - \frac{a^2 \text{Re}(J_{zz})}{\pi^2} \left[ (\partial_x \Phi_+)^2 + (\partial_x \Phi_-)^2 \right] - \frac{a \text{Re}(J_z + \bar{J}_z)}{\pi \sqrt{\pi}} \partial_x \Phi_+ - \frac{2a \text{Im}(\tilde{J} - \frac{J_{zz}}{2\pi^2})}{\sqrt{\pi}} \partial_x \Theta_+ \\
& - \frac{a^2 \text{Im}(J_z + \bar{J}_z)}{\pi} [\partial_x \Theta_+ \partial_x \Phi_+ + \partial_x \Theta_- \partial_x \Phi_-] \\
& + \frac{2 \text{Re}(J_{zz})}{\pi^3} \left[ \cos(2\sqrt{\pi}\Phi_+) + \cos(2\sqrt{\pi}\Phi_-) - \frac{1}{2} \cos(2\sqrt{\pi}\Phi_+) \cos(2\sqrt{\pi}\Phi_-) \right] \\
& + \frac{\text{Re}(J_z - \bar{J}_z)}{\pi^2} \sin(2\sqrt{\pi}\Phi_+) . \tag{B38}
\end{aligned}$$

The operator  $\sin(2\sqrt{\pi}\Phi_+)$  is not allowed by symmetry as discussed in section C. Hence, the lattice model can only realize coupling constants for which this operator has zero amplitude. In the following we will therefore exclude this operator.

The inter-chain hopping

$$\hat{\mathcal{K}}_{l,l+1}^{\text{inter}} = -\frac{1}{2} \left( t^* (\hat{n}_{2,l}, \hat{n}_{1,l+1}) \hat{c}_{1,l}^\dagger \hat{c}_{2,l+1} + t^* (\hat{n}_{1,l}, \hat{n}_{2,l+1}) \hat{c}_{2,l}^\dagger \hat{c}_{1,l+1} + \text{H.c.} \right) \tag{B39}$$

is bosonized by returning to spin language and directly inserting the bosonized expressions for the spin operators, i.e. Eq. (B16), into the spin flip terms. This results in

$$\hat{\mathcal{K}}_{l,l+1}^{\text{inter}} \simeq -\frac{\text{Re}(\tilde{J})}{\pi} \cos(2\sqrt{\pi}\Theta_-) \tag{B40}$$

where we neglected further corrections caused by the gauge function which would only renormalize the prefactor in front of the  $\cos(2\sqrt{\pi}\Theta_-)$ -term but not generate further operator content.

### 3. Bosonization of density-density interactions and complete Hamiltonian

Finally, we consider the onsite and nearest neighbor interaction terms

$$\hat{H}_{\text{int}} = \sum_l \sum_{q=1,2} \left[ \frac{U}{2} : \hat{n}_{q,l} :: \hat{n}_{\bar{q},l} : + V (: \hat{n}_{q,l} :: \hat{n}_{q,l+1} : + : \hat{n}_{q,l} :: \hat{n}_{\bar{q},l+1} :) \right] . \tag{B41}$$

Bosonizing we obtain [57]

$$: \hat{n}_{q,l} :: \hat{n}_{q,l+1} : \simeq -\frac{1}{2\pi^2} + \frac{2a^2}{\pi} (\partial_x \Phi_q)^2 + \frac{1}{2\pi^2} \cos(4\sqrt{\pi}\Phi_q) \tag{B42}$$

$$\begin{aligned}
: \hat{n}_{q,l} :: \hat{n}_{\bar{q},l'} : & \simeq \frac{a^2}{\pi} (\partial_x \Phi_q)(\partial_x \Phi_{\bar{q}}) \\
& + \frac{-1 + 2\delta_{l,l'}}{2\pi^2} \left[ \cos(2\sqrt{\pi}(\Phi_q - \Phi_{\bar{q}})) - \cos(2\sqrt{\pi}(\Phi_q + \Phi_{\bar{q}})) \right] \tag{B43}
\end{aligned}$$

for  $l' = l, l+1$  where we have omitted oscillating contributions. Transforming into '+' and '-' fields this yields

$$\begin{aligned}
\hat{H}_{\text{int}} \simeq & \int dx \left\{ \frac{a}{4\pi} \left[ (U + 6V) (\partial_x \Phi_+)^2 - (U - 2V) (\partial_x \Phi_-)^2 \right] \right. \\
& \left. + \frac{U - 2V}{2\pi^2 a} \left[ -\cos(2\sqrt{\pi}\Phi_+) + \cos(2\sqrt{\pi}\Phi_-) \right] + \frac{V}{\pi^2 a} \cos(2\sqrt{\pi}\Phi_+) \cos(2\sqrt{\pi}\Phi_-) \right\} . \tag{B44}
\end{aligned}$$

We are now in the position to add up all terms and arrive at the Bosonized Hamiltonian

$$\hat{H} \simeq \hat{H}_+ + \hat{H}_- + \hat{H}_{+-} \tag{B45}$$

with

$$\hat{H}_+ = \hat{H}_+^0 + \int dx \left[ A(\partial_x \Theta_+) + B(\partial_x \Phi_+) + \Delta(\partial_x \Theta_+)(\partial_x \Phi_+) + \frac{g_1}{(\pi a)^2} \cos(2\sqrt{\pi}\Phi_+) \right], \quad (\text{B46})$$

$$\hat{H}_- = \hat{H}_-^0 + \int dx \left[ \Delta(\partial_x \Theta_-)(\partial_x \Phi_-) + \frac{g_2}{(\pi a)^2} \cos(2\sqrt{\pi}\Phi_-) + \frac{g_3}{(\pi a)^2} \cos(2\sqrt{\pi}\Theta_-) \right],$$

$$\hat{H}_{+-} = \frac{g_4}{(\pi a)^2} \int dx \cos(2\sqrt{\pi}\Phi_+) \cos(2\sqrt{\pi}\Phi_-), \quad (\text{B47})$$

where  $\hat{H}_\nu^0$  for  $\nu = +, -$  denotes the ordinary Tomonaga-Luttinger Hamiltonian

$$\hat{H}_\nu^0 = \frac{u_\nu}{2\pi} \int dx \left[ K_\nu (\partial_x \Theta_\nu)^2 + \frac{1}{K_\nu} (\partial_x \Phi_\nu)^2 \right]. \quad (\text{B48})$$

We obtain for the Luttinger parameter to lowest order in the interactions

$$K_+ = 2 \left( 1 + \frac{U + 6V - 4 \text{Re}(J_{zz})/\pi}{\pi \text{Re}(\tilde{J} - J_{zz}/2\pi^2)} \right)^{-1/2}, \quad (\text{B49})$$

$$K_- = 2 \left( 1 - \frac{U - 2V + 4 \text{Re}(J_{zz})/\pi}{\pi \text{Re}(\tilde{J} - J_{zz}/2\pi^2)} \right)^{-1/2} \quad (\text{B50})$$

while the velocities for each channel  $\nu = +, -$  are given by

$$u_\nu = a 2\pi \text{Re}(\tilde{J} - J_{zz}/2\pi^2)/K_\nu. \quad (\text{B51})$$

Due to the asymmetry with respect to the Tomonaga-Luttinger basis we get linear couplings in the theory, i.e.

$$A = -\frac{2}{\sqrt{\pi}} \text{Im} \left( \tilde{J} - \frac{J_{zz}}{2\pi^2} \right) \quad (\text{B52})$$

$$B = -\frac{1}{\pi\sqrt{\pi}} \text{Re}(J_z + \bar{J}_z) \quad (\text{B53})$$

$$\Delta = -\frac{a}{\pi} \text{Im}(J_z + \bar{J}_z) \quad (\text{B54})$$

which can be interpreted as chemical potentials for the density and phase-excitations for each sector as well as couplings proportional to the momentum operator of each liquid. The latter implies that we have chosen a reference frame, where the system is not at rest.

The pinning terms that appear in our bosonized theory are given by the following coupling constants in the weak coupling limit

$$\frac{g_1}{a} = \frac{1}{2}(2V - U) + \frac{2}{\pi} \text{Re}(J_{zz}), \quad (\text{B55})$$

$$\frac{g_2}{a} = \frac{1}{2}(U - 2V) + \frac{2}{\pi} \text{Re}(J_{zz}), \quad (\text{B56})$$

$$\frac{g_3}{a} = -\pi \text{Re}(\tilde{J}), \quad (\text{B57})$$

$$\frac{g_4}{a} = V - \frac{\text{Re}(J_{zz})}{\pi}. \quad (\text{B58})$$

It must be noted here that the mapping from bosons to spin operators already implies a finite interaction in terms of  $J_{zz}$ , which is non-zero even for  $\theta = U = V = 0$ . Therefore, the weak-coupling limit is never exact and the actual coupling constant will quantitatively differ from the formulas given above. Nonetheless, the operator content and the qualitative behavior with increasing  $\theta$ ,  $V$  and  $U$  is robust.

### Appendix C: Symmetries

Here we discuss how the symmetry transformations on the lattice Hamiltonian are reflected by symmetry operations on the fields in the bosonization as summarized in Table I. This will be used to identify which operators are allowed or forbidden in the effective field theory Hamiltonian.

Symmetry	Lattice	Bosonic fields
Translation	$\hat{b}_j \rightarrow \hat{b}_{j+1}$	$\hat{\Phi}_+(x) \rightarrow \hat{\Phi}_+(x) + \pi, \hat{\Theta}_+(x) \rightarrow \hat{\Theta}_+(x)$ $\hat{\Phi}_-(x) \rightarrow \hat{\Phi}_-(x), \hat{\Theta}_-(x) \rightarrow \hat{\Theta}_-(x)$
Time reversal $\mathcal{K}$	$\hat{b}_j \rightarrow \hat{b}_j$	$\hat{\Phi}_+(x) \rightarrow \hat{\Phi}_+(x), \hat{\Theta}_+(x) \rightarrow -\hat{\Theta}_+(x)$ $\hat{\Phi}_-(x) \rightarrow \hat{\Phi}_-(x), \hat{\Theta}_-(x) \rightarrow -\hat{\Theta}_-(x)$
$U(1)$ gauge	$\hat{b}_j \rightarrow \hat{b}_j e^{i\alpha}$	$\hat{\Phi}_+(x) \rightarrow \hat{\Phi}_+(x), \hat{\Theta}_+(x) \rightarrow \hat{\Theta}_+(x) + \alpha$ $\hat{\Phi}_-(x) \rightarrow \hat{\Phi}_-(x), \hat{\Theta}_-(x) \rightarrow \hat{\Theta}_-(x)$
Site parity $\mathcal{I}_-$	$\hat{b}_j \rightarrow \hat{b}_{-j}$	$\hat{\Phi}_+(x) \rightarrow -\hat{\Phi}_+(-x) + \pi, \hat{\Theta}_+(x) \rightarrow \hat{\Theta}_+(-x)$ $\hat{\Phi}_-(x) \rightarrow -\hat{\Phi}_-(-x), \hat{\Theta}_-(x) \rightarrow \hat{\Theta}_-(-x)$
Link parity $\mathcal{I}$	$\hat{b}_j \rightarrow \hat{b}_{1-j}$	$\hat{\Phi}_+(x) \rightarrow -\hat{\Phi}_+(-x), \hat{\Theta}_+(x) \rightarrow \hat{\Theta}_+(-x)$ $\hat{\Phi}_-(x) \rightarrow -\hat{\Phi}_-(-x), \hat{\Theta}_-(x) \rightarrow \hat{\Theta}_-(-x)$

TABLE I: Symmetry operations and their realizations in Bosonic fields.

The anyonic lattice model of interest  $\hat{H} = \hat{H}_{\text{kin}} + \hat{H}_{\text{int}}$  with

$$\hat{H}_{\text{kin}} = -J \sum_l \left[ \hat{b}_l^\dagger \hat{b}_{l+1} e^{i\theta \hat{n}_l} + \text{H.c.} \right] \quad (\text{C1})$$

$$\hat{H}_{\text{int}} = \sum_l \left[ \frac{U}{2} \hat{n}_l (\hat{n}_l - 1) + V \hat{n}_l \hat{n}_{l+1} \right] \quad (\text{C2})$$

exhibits translational invariance and conservation of total particle number ( $U(1)$  gauge). Link reflection symmetry  $\mathcal{I}$  and time-reversal  $\mathcal{K}$ , in contrast, are broken. All symmetries are inherited by the Bosonic low-energy description and Table I summarizes their realizations.

A modified inversion symmetry is still obeyed [8]. The lattice model is invariant under the combined symmetry operation  $\tilde{\mathcal{I}} = \hat{U}(\theta) \mathcal{K} \mathcal{I}$  where the non-linear unitary transformation  $\hat{U}(\theta) = e^{-i\theta \sum_l \hat{n}_l (\hat{n}_l - 1)/2}$  generates a density-dependent phase for Bosonic operators [8]

$$\hat{b}_l^\dagger \rightarrow \hat{U}(\theta) \hat{b}_l^\dagger \hat{U}^\dagger(\theta) = \hat{b}_l^\dagger e^{-i\theta \hat{n}_l} . \quad (\text{C3})$$

While the realizations of  $\mathcal{K}$  and  $\mathcal{I}$  are known, see Table I, it is difficult to determine how the transformation  $\hat{U}(\theta)$  acts on the Bosonic fields. This is due to the fact that the density dependent phase  $\exp(-i\theta \hat{n}_l)$  is represented by integer values of  $n_l$  on the lattice, which ensures a  $\theta \rightarrow \theta + 2\pi$  periodicity. In the continuum limit there is no such lattice restriction, so it is far from trivial to implement shifts of the fields that have this topological property. From Eq. (C3) and section A we know that  $\hat{U}(\theta)$  generates factors of the form as in Eq. (A2) above which can be absorbed by redefinition of the coefficients  $a(\theta)$  and  $b(\theta)$  which in turn determine the coupling constants  $\tilde{J}, J_z, \bar{J}_z$  and  $J_{zz}$  of the spin-1/2 two-leg ladder model. Such non-linear transformations cannot be tracked in the bosonized expressions of  $\hat{S}_{q,l}^\pm$  in Eq. (B16) and therefore the realization of the combined symmetry operation  $\hat{U}(\theta) \mathcal{K} \mathcal{I}$  in  $\Theta_\pm$  is unclear.

On the other hand, it is clear that densities  $\hat{b}_l^\dagger \hat{b}_l = \hat{n}_l = -\hat{S}_{1,l}^z - \hat{S}_{2,l}^z + 1$  are not affected by  $\hat{U}(\theta)$ , so therefore any transformation on the fields due to  $\hat{U}(\theta)$  must also leave the spin-z operators in Eq. (B15) invariant. Therefore, shifts on the  $\Phi$ -fields cannot be generated by  $\hat{U}(\theta)$ , while we cannot make any statement how the  $\Theta$ -fields are transformed.

Next, we turn to the modified inversion symmetry which is represented by the combined symmetry operation  $\tilde{\mathcal{I}} = \hat{U}(\theta) \mathcal{K} \mathcal{I}$ . For densities in Eq. (B15) this operation corresponds to a simple inversion symmetry  $S_{q,l}^z \rightarrow S_{q,1-l}^z$ , since  $\mathcal{K}$  and  $\hat{U}(\theta)$  do not affect the densities. We therefore conclude that the Bosonic  $\Phi$ -fields transform as

$$\Phi_q(x) \rightarrow -\Phi_q(-x) \quad q = 1, 2 \quad (\text{C4})$$

and

$$\Phi_+(x) \rightarrow -\Phi_+(-x), \quad \Phi_-(x) \rightarrow -\Phi_-(-x) \quad (\text{C5})$$

under the action of the combined symmetry  $\hat{U}(\theta) \mathcal{K} \mathcal{I}$ . Even without knowing the symmetry action on the  $\Theta$ -fields, the transformation property of  $\Phi_+(x)$  in Eq. (C5) rules out the existence of the  $\sin(\sqrt{4\pi} \Phi_+(x))$  - operator as a perturbation. Note, that the operators  $\Delta \partial_x \Theta_\pm(x) \partial_x \Phi_\pm(x)$  appearing in the bosonized anyonic Hamiltonian in Eq. (7) of the main text obey the combined  $\mathcal{K} \mathcal{I}$  symmetry, i.e.  $\hat{\Phi}_\pm(x) \rightarrow -\hat{\Phi}_\pm(-x)$  and  $\hat{\Theta}_\pm(x) \rightarrow -\hat{\Theta}_\pm(-x)$ , see Table I.

### Appendix D: Additional numerical data for order parameters, fidelity susceptibility, entanglement entropy, and correlation lengths

In Figs. 5-9 additional numerical data for the order parameters, the fidelity susceptibility, the entanglement entropy and the correlation length across phase transition lines is presented to illustrate how the phase transition lines were determined and analyzed. In addition to the order parameters as shown in Fig. 5, we used the fidelity susceptibility in Figs. 6 and 7 and the entangle entropy in Figs. 8 and 9. We will define and explain those quantities in the following.

A special property of one-dimensional, gapped Hamiltonians can be conveniently formalized by means of the entanglement entropy. The quantity is defined as the Von Neumann entropy, i.e.

$$S(\hat{\rho}) = -\text{tr}\hat{\rho}\ln(\hat{\rho}) \quad (\text{D1})$$

of the so-called reduced density matrix  $\hat{\rho} \equiv \hat{\rho}_{R,L}$ , obtainable by partially tracing out a sub-system from the pure density matrix,

$$\hat{\rho}_{R,L} = \text{tr}_{L,R}\hat{\rho}. \quad (\text{D2})$$

The entanglement entropy in Eq. (D1) is thereby equivalent for each  $L, R$  following from the Schmidt decomposition of an arbitrary pure state into two orthonormal bases.  $S(\rho_{L,R}) \geq 0$  quantifies how entangled the two subsystems are, with  $S(\rho_{L,R}) = 0$  denoting the special case that both sub-systems are in product form, and fully unentangled.

The von Neumann entanglement entropy diverges logarithmically in the correlation length  $\xi$  when approaching a critical point [44], i.e.

$$S(\rho_{L,R}) \propto c \ln(\xi) \quad (\text{D3})$$

with  $c$  being the central charge of the underlying two-dimensional conformal field theory. For finite size systems the correlation length at the continuous transition is limited by the system size  $L$ . At the critical point, the entanglement entropy then diverges as

$$S(\rho_{L,R}) = \frac{c}{6} \ln(L) \quad (\text{D4})$$

where the factor  $1/6$  applies to open boundary conditions [44].

Another useful quantity to observe the occurrence of phase transitions in the framework of DMRG is the fidelity of quantum states  $F$  and especially its susceptibility  $\chi$ . The fidelity is defined as the absolute value of the overlap between a quantum state  $|\Psi(\lambda)\rangle$  depending on a parameter  $\lambda$  with a state with a slightly shifted parameter  $|\Psi(\lambda + \delta\lambda)\rangle$ , i.e.

$$F = |\langle\Psi(\lambda)|\Psi(\lambda + \delta\lambda)\rangle|. \quad (\text{D5})$$

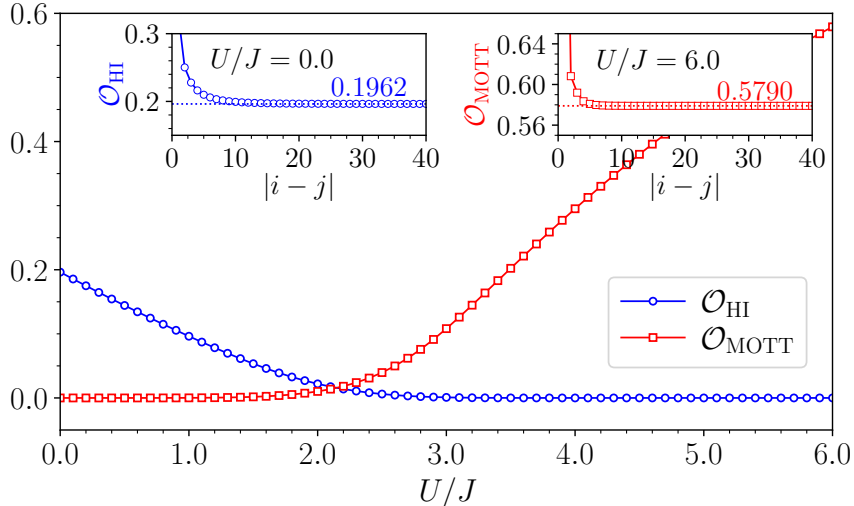


FIG. 5: String order parameters  $\mathcal{O}_{\text{HI}}$  and  $\mathcal{O}_{\text{Mott}}$  plotted along the HI to Mott transition as a function of  $U/J$ , showing the existing hidden order in both phases at  $V/J = 1.0, \theta = 0$ . The insets show how the values were obtained at example points deep in the phases at  $U/J = 0.0$  (HI phase) and  $U/J = 6.0$  (Mott phase) respectively.  $\mathcal{O}(|i-j|)$  is extrapolated to  $|i-j| \rightarrow \infty$  marked by the dotted lines. Data shown from finite DMRG,  $L = 100, M = 400$ , periodic boundary conditions.

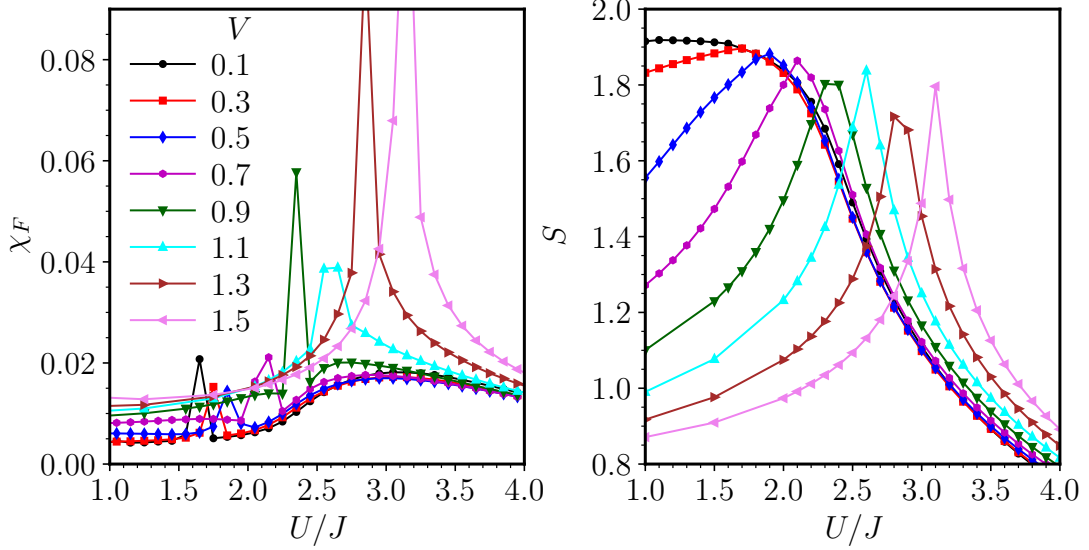


FIG. 6: Fidelity susceptibility  $\chi_F$  (left) and entanglement entropy  $S$  (right) plotted over  $U/J$  across the Mott to HI transition for  $\theta = 0$  and various fixed values of  $V/J$ . Data shown from iDMRG,  $M = 400$ .

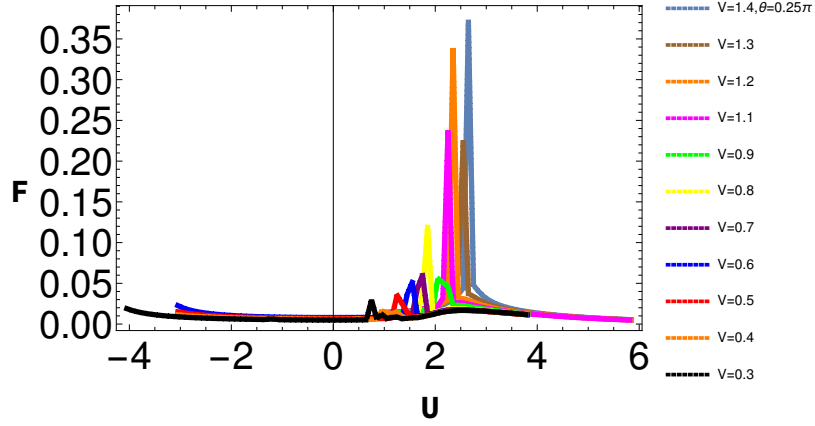


FIG. 7: Fidelity susceptibility  $\chi_F$  for  $\theta = 0.25$  plotted over  $U/J$  across the Mott to HI transition for various fixed values of  $V/J$ . Data shown from iDMRG,  $M = 400$ .

It is convenient to define its logarithmic derivative,

$$\chi_F = -\left. \frac{\partial^2 \ln(F)}{\partial \delta \lambda^2} \right|_{\delta \lambda=0}. \quad (\text{D6})$$

Here, the parameter  $\lambda$  is the free parameter along which line the phase transition is to be located.

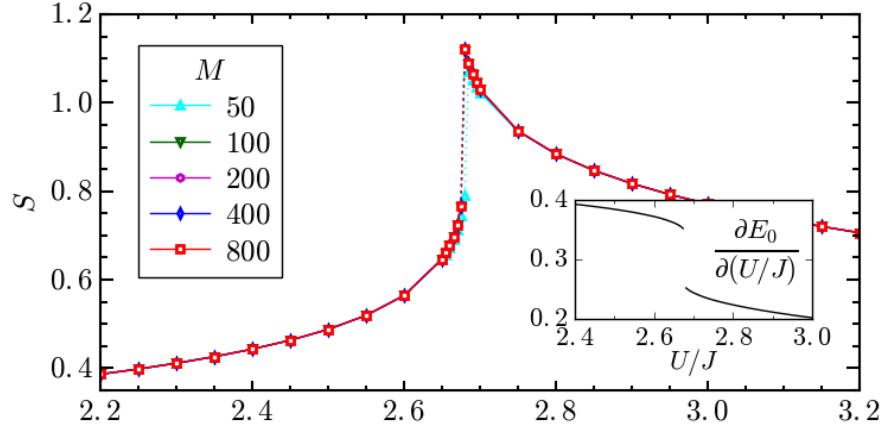


FIG. 8: Entanglement entropy  $S$  (large plot) and partial derivative of ground-state energy with  $U/J$  (inlet) plotted over  $U/J$  at fixed  $V/J = 3.0, \theta = \pi$  across the CDW to Mott transition line. Both quantities show a jump characteristic of a 1st order transition. Data from iDMRG,  $M = 50$  to  $M = 800$  to exclude the possibility of an accuracy error.

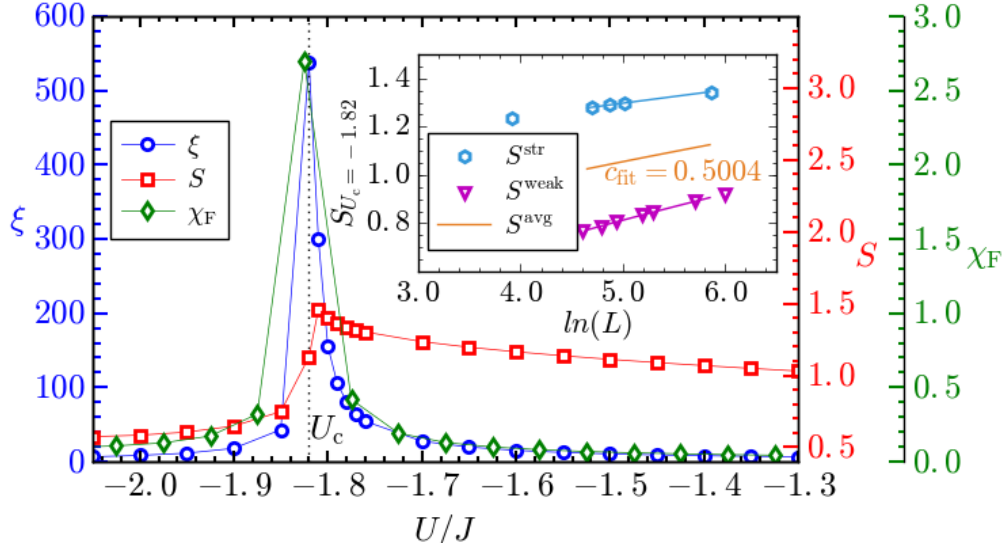


FIG. 9: Correlation length  $\xi$ , entanglement entropy  $S$  and fidelity susceptibility  $\chi_F$  plotted over  $U/J$  along the dimer to Mott transition line at  $V/J = 0.2, \theta = \pi$  showing a 2nd order transition at  $U_c/J = -1.82$ . Data from iDMRG,  $M = 800$ . Inlet shows entanglement entropy at the transition point  $V/J = 0.2, U_c/J = -1.82$  plotted over  $\ln(L)$ , the slope of which is given by  $c/6$ . Depending on the cut being along a strong or weak bond, we get  $S^{\text{str}}$  and  $S^{\text{weak}}$ . The slope of the averaged entropy  $S^{\text{avg}}$  corresponds to a central charge  $c = 0.5004$ . Inlet data from DMRG with  $M = 400$  using open boundary conditions,  $S$  measured on middle bond for minimal boundary effect.

- [1] J. Leinaas and J. Myrheim, On the theory of identical particles, *Nuovo Cimento Soc. Ital. Fis.* **37B**, 1 (1977).  
 [2] In the original paper [1] fractional statistics for both two-dimensional and one-dimensional geometries are discussed. Our work refers to the 1D case.  
 [3] A. Eckardt, Colloquium: Atomic quantum gases in periodically driven optical lattices, *Rev. Mod. Phys.* **89**,

- 011004 (2017).  
 [4] N. Goldman and J. Dalibard, Periodically driven quantum systems: Effective Hamiltonians and engineered gauge fields, *Phys. Rev. X* **4**, 031027 (2014).  
 [5] M. Bukov, L. D'Alessio, and A. Polkovnikov, Universal high-frequency behavior of periodically driven systems: from dynamical stabilization to Floquet engineering, *Ad-*



- vances in Physics **64**, 139 (2015).
- [6] T. Keilmann, S. Lanzmich, I. McCulloch, and M. Roncaglia, Statistically induced phase transitions and anyons in 1D optical lattices, *Nature Communications* **2**, 361 EP (2011), article.
- [7] S. Greschner and L. Santos, Anyon Hubbard model in one-dimensional optical lattices, *Phys. Rev. Lett.* **115**, 053002 (2015).
- [8] F. Lange, S. Ejima, and H. Fehske, Anyonic Haldane insulator in one dimension, *Phys. Rev. Lett.* **118**, 120401 (2017).
- [9] C. Sträter, S. C. L. Srivastava, and A. Eckardt, Floquet realization and signatures of one-dimensional anyons in an optical lattice, *Phys. Rev. Lett.* **117**, 205303 (2016).
- [10] G. Tang, S. Eggert, and A. Pelster, Ground-state properties of anyons in a one-dimensional lattice, *New Journal of Physics* **17**, 123016 (2015).
- [11] F. Lange, S. Ejima, and H. Fehske, Strongly repulsive anyons in one dimension, *Phys. Rev. A* **95**, 063621 (2017).
- [12] F. Liu, J. R. Garrison, D.-L. Deng, Z.-X. Gong, and A. V. Gorshkov, Asymmetric particle transport and light-cone dynamics induced by anyonic statistics, *Phys. Rev. Lett.* **121**, 250404 (2018).
- [13] M. Bonkhoff, K. Jägering, S. Eggert, A. Pelster, M. Thorwart, and T. Posske, Bosonic continuum theory of one-dimensional lattice anyons, *Phys. Rev. Lett.* **126**, 163201 (2021).
- [14] M. Bonkhoff, S. B. Jäger, I. Schneider, A. Pelster, and S. Eggert, Coherence properties of the repulsive anyon-Hubbard dimer, *Phys. Rev. B* **108**, 155134 (2023).
- [15] F. Görg, K. Sandholzer, J. Minguzzi, R. Desbuquois, M. Messer, and T. Esslinger, Realization of density-dependent Peierls phases to engineer quantized gauge fields coupled to ultracold matter, *Nat. Phys.* **15**, 1161 (2019).
- [16] V. Lienhard, P. Scholl, S. Weber, D. Barredo, S. de Léséleuc, R. Bai, N. Lang, M. Fleischhauer, H. P. Büchler, T. Lahaye, and A. Browaeys, Realization of a density-dependent Peierls phase in a synthetic, spin-orbit coupled Rydberg system, *Phys. Rev. X* **10**, 021031 (2020).
- [17] J. Kwan, P. Segura, Y. Li, S. Kim, A. V. Gorshkov, A. Eckardt, B. Bakka-Hassani, and M. Greiner, Realization of 1D anyons with arbitrary statistical phase, arXiv:2306.01737 <https://doi.org/10.48550/arXiv.2306.01737>.
- [18] I. Bloch, J. Dalibard, and W. Zwerger, Many-body physics with ultracold gases, *Rev. Mod. Phys.* **80**, 885 (2008).
- [19] M. Aidelsburger, M. Atala, M. Lohse, J. T. Barreiro, B. Paredes, and I. Bloch, Realization of the Hofstadter Hamiltonian with ultracold atoms in optical lattices, *Phys. Rev. Lett.* **111**, 185301 (2013).
- [20] H. Miyake, G. A. Siviloglou, C. J. Kennedy, W. C. Burton, and W. Ketterle, Realizing the Harper Hamiltonian with laser-assisted tunneling in optical lattices, *Phys. Rev. Lett.* **111**, 185302 (2013).
- [21] J. Struck, M. Weinberg, C. Ölschläger, P. Windpassinger, J. Simonet, K. Sengstock, R. Höppner, P. Hauke, A. Eckardt, M. Lewenstein, and L. Mathey, Engineering Ising-XY spin-models in a triangular lattice using tunable artificial gauge fields, *Nature Physics* **9**, 738–743 (2013).
- [22] S. Fazzini, P. Chudzinski, C. Dauer, I. Schneider, and S. Eggert, Nonequilibrium Floquet steady states of time-periodic driven Luttinger liquids, *Phys. Rev. Lett.* **126**, 243401 (2021).
- [23] C. Schweizer, F. Grusdt, M. Berngruber, L. Barbiero, E. Demler, N. Goldman, I. Bloch, and M. Aidelsburger, Floquet approach to Z2 lattice gauge theories with ultracold atoms in optical lattices, *Nature Physics* **15**, 1168 (2019).
- [24] T. Langen, R. Geiger, and J. Schmiedmayer, Ultracold atoms out of equilibrium, *Annual Review of Condensed Matter Physics* **6**, 201 (2015).
- [25] C. Gross and I. Bloch, Quantum simulations with ultracold atoms in optical lattices, *Science* **357**, 995 (2017).
- [26] A. Frölian, C. S. Chisholm, E. Neri, C. R. Cabrera, R. Ramos, A. Celi, and L. Tarruell, Realizing a 1D topological gauge theory in an optically dressed BEC, *Nature* **608**, 293 (2022).
- [27] C. S. Chisholm, A. Frölian, E. Neri, R. Ramos, L. Tarruell, and A. Celi, Encoding a one-dimensional topological gauge theory in a Raman-coupled Bose-Einstein condensate, *Phys. Rev. Res.* **4**, 043088 (2022).
- [28] M. Nakamura, Mechanism of CDW-SDW transition in one dimension, *Journal of the Physical Society of Japan* **68**, 3123 (1999), <https://doi.org/10.1143/JPSJ.68.3123>.
- [29] P. Sengupta, A. W. Sandvik, and D. K. Campbell, Bond-order-wave phase and quantum phase transitions in the one-dimensional extended Hubbard model, *Phys. Rev. B* **65**, 155113 (2002).
- [30] A. W. Sandvik, L. Balents, and D. K. Campbell, Ground state phases of the half-filled one-dimensional extended Hubbard model, *Phys. Rev. Lett.* **92**, 236401 (2004).
- [31] L. Barbiero, S. Fazzini, and A. Montorsi, Non-local order parameters as a probe for phase transitions in the extended Fermi-Hubbard model, *Eur. Phys. J. Spec. Top.* **226**, 2697 (2017).
- [32] E. G. Dalla Torre, E. Berg, and E. Altman, Hidden order in 1D Bose insulators, *Phys. Rev. Lett.* **97**, 260401 (2006).
- [33] E. Berg, E. G. Dalla Torre, T. Giamarchi, and E. Altman, Rise and fall of hidden string order of lattice bosons, *Phys. Rev. B* **77**, 245119 (2008).
- [34] S. Ejima, F. Lange, and H. Fehske, Spectral and entanglement properties of the bosonic Haldane insulator, *Phys. Rev. Lett.* **113**, 020401 (2014).
- [35] D. Rossini and R. Fazio, Phase diagram of the extended Bose-Hubbard model, *New Journal of Physics* **14**, 065012 (2012).
- [36] M. Dalmonte, M. Di Dio, L. Barbiero, and F. Ortolani, Homogeneous and inhomogeneous magnetic phases of constrained dipolar bosons, *Phys. Rev. B* **83**, 155110 (2011).
- [37] H. J. Schulz, Phase diagrams and correlation exponents for quantum spin chains of arbitrary spin quantum number, *Phys. Rev. B* **34**, 6372 (1986).
- [38] In the Appendix details about the lattice gauge function, about bosonization, about symmetry transformations, and additional numerical data are presented.
- [39] P. Lecheminant, A. O. Gogolin, and A. A. Nersisyan, Criticality in self-dual sine-Gordon models, *Nuclear Physics B* **639**, 502 (2002).
- [40] S. R. White, Density matrix formulation for quantum renormalization groups, *Phys. Rev. Lett.* **69**, 2863 (1992).
- [41] S. R. White, Density-matrix algorithms for quantum

- renormalization groups, *Phys. Rev. B* **48**, 10345 (1993).
- [42] I. P. McCulloch, Infinite size density matrix renormalization group, revisited (2008), [arXiv:0804.2509](https://arxiv.org/abs/0804.2509) [[cond-mat.str-el](https://arxiv.org/abs/0804.2509)].
- [43] T. Ogino, S. Furukawa, R. Kaneko, S. Morita, and N. Kawashima, Symmetry-protected topological phases and competing orders in a spin- $\frac{1}{2}$  xxz ladder with a four-spin interaction, *Phys. Rev. B* **104**, 075135 (2021).
- [44] S. Nishimoto, Tomonaga-Luttinger-liquid criticality: Numerical entanglement entropy approach, *Phys. Rev. B* **84**, 195108 (2011).
- [45] R. A. Macêdo, F. B. Ramos, and R. G. Pereira, Continuous phase transition from a chiral spin state to collinear magnetic order in a zigzag chain with Kitaev interactions, *Phys. Rev. B* **105**, 205144 (2022).
- [46] C. Mudry, A. Furusaki, T. Morimoto, and T. Hikihara, Quantum phase transitions beyond Landau-Ginzburg theory in one-dimensional space revisited, *Phys. Rev. B* **99**, 205153 (2019).
- [47] S. Jiang and O. Motrunich, Ising ferromagnet to valence bond solid transition in a one-dimensional spin chain: Analogies to deconfined quantum critical points, *Phys. Rev. B* **99**, 075103 (2019).
- [48] R.-Z. Huang, D.-C. Lu, Y.-Z. You, Z. Y. Meng, and T. Xi-ang, Emergent symmetry and conserved current at a one-dimensional incarnation of deconfined quantum critical point, *Phys. Rev. B* **100**, 125137 (2019).
- [49] B. Roberts, S. Jiang, and O. I. Motrunich, Deconfined quantum critical point in one dimension, *Phys. Rev. B* **99**, 165143 (2019).
- [50] Q. Luo, S. Hu, J. Li, J. Zhao, H.-Y. Kee, and X. Wang, Spontaneous dimerization, spin-nematic order, and deconfined quantum critical point in a spin-1 Kitaev chain with tunable single-ion anisotropy, *Phys. Rev. B* **107**, 245131 (2023).
- [51] C. Zhang and M. Levin, Exactly solvable model for a deconfined quantum critical point in 1D, *Phys. Rev. Lett.* **130**, 026801 (2023).
- [52] T. Senthil, L. Balents, S. Sachdev, A. Vishwanath, and M. P. A. Fisher, Quantum criticality beyond the Landau-Ginzburg-wilson paradigm, *Phys. Rev. B* **70**, 144407 (2004).
- [53] M. Levin and T. Senthil, Deconfined quantum criticality and néel order via dimer disorder, *Phys. Rev. B* **70**, 220403 (2004).
- [54] C. Wang, A. Nahum, M. A. Metlitski, C. Xu, and T. Senthil, Deconfined quantum critical points: Symmetries and dualities, *Phys. Rev. X* **7**, 031051 (2017).
- [55] L. Landau and E. Lifshitz, *Statistical Physics, Part I, Vol.5* (Elsevier Butterworth-Heinemann, Oxford, 1980).
- [56] S. Ejima and H. Fehske, Comparative density-matrix renormalization group study of symmetry-protected topological phases in spin-1 chain and Bose-Hubbard models, *Phys. Rev. B* **91**, 045121 (2015).
- [57] T. Giamarchi, *Quantum Physics in One Dimension* (Clarendon Press, 2003).